

## Static and dynamic axial crushing of prismatic thin-walled metal columns

Ahmad Malekshahi<sup>a,\*</sup>, Kouros Heidari Shirazi<sup>a</sup> and Mohammad Shishesaz<sup>a</sup>

<sup>a</sup>Department of Mechanical Engineering, Shahid Chamran University of Ahvaz, Ahvaz, Iran

### ARTICLE INFO

#### Article history:

Received

Received in revised form

Accepted

Available online

#### Keywords:

Progressive collapse

mean crushing force

axial impact

crushing wavelength

LS-DYNA

### ABSTRACT

In this paper, a novel approach is proposed to investigate the progressive collapse damage of prismatic thin walled metal columns with different regular cross sections, under the action of axial quasi-static and impact loads. The present work mainly focuses on implementation of some important factors which have been neglected in other studies. These factors include the effect of reducing impactor velocity and inertia effect during collapse, a mixed collapse mode for crushing mechanism, and consideration of a realistic elasto-plastic model for material. Taking all these factors into account, the analysis led to some parametric algebraic equations without a possible general solution in terms of collapse variables. Consequently, a new theoretical approach was proposed based on previously offered Super Folding Element (SFE) theory, to obtain the closed form explicit relations for the static and dynamic mean crushing forces and collapse variables. The proposed approach considers an analytic-numeric discretization procedure to solve these equations. To evaluate the results, a detailed finite element analysis on square mild steel models was conducted under an axial impact load, using LS-DYNA and ANSYS software programs. Comparison of the experimental results that are available in the literature with those of finite element analysis, shows the applicability of this approach in predicting the collapse behavior in such structures.

### 1. Introduction

Thin walled metal structures, due to their high strength to weight ratio, have numerous applications in different engineering fields. For many years, metallic components have been used for carrying load and improving the *crashworthiness* of composite *transportation* structures in terms of absorbing the impact energy in aircrafts, ships, and road/rail vehicles. Since crashworthiness relates to human safety and protecting against accidents, the design qualifications become an important issue in design of such structures. As a result, before taking any steps, it is important to analyze the simple geometries in the shortest time possible with the least design costs.

One of the main issues to be considered during crushing or collapse analysis of thin walled metal columns, is the evaluation of energy absorption capacity of the whole structure experiencing the impact or quasi-static load. Despite its importance, crushing analysis has not been sufficiently addressed for some reasons; first,

most structures are primarily designed to function in elastic loading range and beyond that, they lose their efficiency and secondly, the collapse phenomenon includes large deformations with nonlinear and uncertain complicated equations which makes the analysis very cumbersome and expensive. In such cases, a closed form solution is usually out of reach. One of the logical ways to handle such problems is to use the available finite element codes, such as LS-DYNA solver, or any other similar software.

Owing to this fact, the axial collapse of thin-walled structures that has been addressed by many researchers can be generally categorized in different groups, based on the type of applied load (i.e. quasi-static and impact), or shape of the structure (i.e. single-cell, multi-cell and foam filled). In addition, numerical, analytical, and/or experimental methods (or a combination of each method) may have been used in each study group. Some researchers have investigated crushing behavior of thin walled structures under quasi-static loading [1-15] while others, have implemented a

\* Corresponding Author. Tel.: +98-613-333-0010-20; fax: +98-613-333-6642. Email Address: [a-malekshahi@phdstu.scu.ac.ir](mailto:a-malekshahi@phdstu.scu.ac.ir)

dynamic or impact load [16-27] in their analyses. Some scientists have explored the crashworthiness design of these structures [28-31], while others have used new materials (composites, nano or FG materials) or foam filled structures to improve their design performance [32-34].

Alexander [1] was one of the first ones to present a theoretical approach for prediction of mean crushing force in thin walled cylindrical metal columns, collapsing under quasi-static loads. Although his model was very simple but still could predict mean crushing force very well. Later on, Wierzbicki and Abramowicz [2], as well as Jones and Abramowicz [3] carried out some analytical studies on axial collapse of metal columns under a quasi-static load. They introduced a theory and named it as Super Folding Element (SFE) which is an approach for estimating the mean crushing force in thin walled members. Based on this theory, instead of solving the complicated governing differential equations for shell deformation, the absorbed energy could be estimated in certain areas of the shell which undergo large plastic deformations. Implementing this method and selecting an appropriate constitutive element and suggesting some collapse modes based on experimental observations, they derived relations for the absorbed energy during collapse. Their predictions were relatively in good agreement with experimental results. In a later study, Abramowicz and Wierzbicki [4], improved the predictions of their preceding studies by combining two different collapse (crushing) modes. These modes which were identified as a quasi-inextensional collapse mode followed by an extensional mode took place successively during crushing process. Other researches such as White et al. [5] and Najafi and Rais-Rohani [6], used this method to predict mean crushing force for different geometries. Hao et al. [7] conducted a theoretical study to predict the progressive buckling and energy absorption of the sinusoidal corrugated tubes subjected to axial crushing. Hong et. al [8] carried out some experiments to evaluate deformation curves and collapse modes of triangular steel tubes under quasi-static axial compression. The energy absorption capacity of axially compressed expanded metal tubes was investigated by Martínez et al. [9]. They validated their numerical results with those of nonlinear finite element findings and experimental results. In other similar studies, Wierzbicki and Abramowicz [10] investigated the mechanics of deep plastic collapse of thin walled structures while, Zhang and Huh [11], worked on crushing analysis of polygonal columns and angle elements. Zhang and Huh [12], analyzed crush resistance of square tubes with various thickness configurations, and Song et. al [13] sought a relationship between progressive collapse and initial buckling for tubular structures under axial loading. Crushing behavior of multi-cell or honeycombs was also studied by others [14, 15].

There are also some other studies that have investigated the axial collapse of columns under an impact load using finite element or experimental methods (or combination of both). The first study in this field was reported by Macaulay and Redwood [16] on small scale model of railway coaches under impact. Pugsley [17] studied crumpling of aluminum tubular structures under impact loads. In a separate work, Coppa [18] investigated the new ways to attenuate shock loads emanating from impact loads. Ezra and Fay [19] assessed energy absorbing devices for prospective use in aircrafts under impact loads, while, Reid and Reddy [20] studied the use of metallic tubes as impact energy absorbers. However the more recent investigations on this topic were carried out by Abramowicz and Jones [21], as well as Abramowicz [22], on dynamic progressive buckling of circular and square tubes. They proposed an efficient theoretical approach and carried out some experimental tests on square and circular

mild steel samples under axial impact. They measured the mean crushing force and overall crushing distance by observing the collapse modes of the crushed samples. Furthermore, following the Wierzbicki and Abramowicz approach, they derived relations for dynamic mean crushing force. In spite of a relatively fair agreement between their experimental and analytical results which were based on the same model, they did not include some of the important factors such as mixed collapse mode or realistic elasto-plastic model of the material, and even the effect of reducing impactor velocity in their analysis. Recent studies on crushing behavior of structures have focused on crashworthiness design [28-31] under the action of an impact load. These studies are usually cumbersome and computationally expensive and need a fast computer and proper finite element software to seek a solution. There are also some new investigations in the literature considering the application of new materials (or nano-materials) [33], foams [34, 35], composite or FGM [36], to investigate their buckling behavior and/or degree of the absorbed energy during this process.

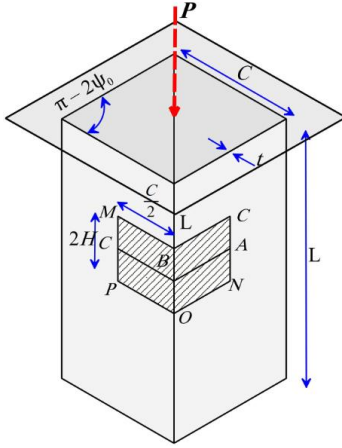
The main goal in present research is to obtain a meaningful relation between the crushing force and axial collapse variables of prismatic metal columns with regular sectional shapes, based on a model in which other essential factors neglected by other researches have been included in the analysis. These essential factors include the effect of reducing impactor velocity and inertia effect during collapse, a mixed collapse mode for crushing mechanism, and consideration of a realistic elasto-plastic model for material under an axial load (static and dynamic). The proposed approach which is based on SFE theory, is capable of predicting static and dynamic mean crushing forces, as well as collapse variables (crushing wavelength  $2H$  and curvature radius  $b$ ), by considering all important aspects in modeling which have been neglected so far. The study first determines the maximum or peak force using a method called direct strength method (DSM). This method offers an efficient approach which has already been used (Refs. [37, 38]) in thin walled metal structures to obtain their load carrying capacity. As the second step, using SFE theory in the post-buckling regime, the internal energy due to axial collapse is calculated. This energy is obtained for each crushing wavelength based on the deformation or crushing mode of an angle element, as a constitutive element extracted from the column walls. Balancing the resulting internal energy with the external work, the mean crushing force is extracted. In the next step, using the optimality conditions for the crushing forces with respect to the collapse variables, a set of nonlinear algebraic equations are obtained which lack a general analytic solution. One of the novelties of the present work is to propose a semi-analytical procedure to find a general solution to these equations. This approach uses a discretization procedure for solving parametric equations to yield the explicit relations for crushing force and collapse variables. In the case of impact loading, the effects of strain rate and reduction of the impactor velocity during progressive collapse is considered such that instead of using just one crushing force during the whole collapse regime (as in previous studies), a progressively decaying crushing force is obtained for each crushing wavelength. To evaluate the results, a detailed step by step finite element study is performed using LS-DYNA solver for simulating the crushing process on a variety of square mild steel samples. At last, the results of the proposed model (and approach) will be discussed and compared with those reported by experimental work of others, and that of finite element study also performed in this work.

## 2. Theoretical approach

### 2.1. Buckling analysis

Consider a typical thin-walled metal column sustaining an axial force  $P$  and geometrical parameters shown in Fig. 1. Using direct strength method and calibration with experimental data, Schafer [37, 38] showed that the ultimate local buckling load for such column is defined as follows:

$$P_{ult} = \begin{cases} \left(1 - 0.15 \left(\frac{P_{cr}}{P_Y}\right)^{0.4}\right) \left(\frac{P_{cr}}{P_Y}\right)^{0.4} P_Y & \text{for } \sqrt{\frac{P_{cr}}{P_Y}} < 0.776 \\ P_Y & \text{other values} \end{cases} \quad (1)$$



**Figure 1.** A typical thin-walled metal column with given dimensions under an axial load.

where  $P_{cr}$  and  $P_Y$  are the critical and yield loads corresponding to the critical and yield stresses defined in Eqs. (2) and (3) [37, 38].

$$P_{cr} = A_g \left( \frac{k_c \pi^2 E}{12(1-\nu^2)} \left( \frac{t}{C} \right)^2 \right) \quad (2)$$

$$P_Y = A_g \sigma_Y \quad (3)$$

In these equations,  $A_g$  is the gross cross sectional area of the column and  $k_c$  is the buckling coefficient for the column wall (plates). It is assumed that a linear load path exists until the collapse, while each plate experiences simply supported boundary conditions ( $k_c \cong 4$ ) [39], irrespective of the connecting angle between the plates. This assumption was confirmed by findings on linear buckling analysis performed by FEM. Therefore the absorbed elastic energy by the column before collapse is estimated as follows [39]:

$$E_0 = \frac{P_{ult}^2 L}{2EA_g} \quad (4)$$

Note that Eqs. (1) and (4) are reliable for quasi-static loading. For the impact loading, these equations are multiplied by a factor related to strain rate effects which will be presented later. It is worth to mention that in previous studies, the energy  $E_0$  has been excluded from the plastic energy during crushing process. The present work will include this term, as will be shown in the following section.

### 2.2. Collapse analysis

After the column has reached its ultimate load carrying capacity  $P_{ult}$ , it collapses and then the energy is absorbed through

large plastic deformation. A corner element cut out from the column sidewalls with geometrical parameters shown in Fig. 1, is used as the base element in collapse analysis. Based on the experimental observations reported by [2-4], there are two crushing mechanisms known as collapse modes which take place simultaneously. These two modes are named as quasi-inextensional mode (shown in Fig. 2(a)) and extensional collapse mode (shown in Fig. 2(b)). In this work, it is assumed that the collapse is progressive and takes place in a sequential manner for each folding element. In other words, the collapse begins with a quasi-inextensional mode and then progresses to an intermediate configuration  $\bar{\alpha}$  (also known as switching angle). The latter mode is followed by the extensional mode which takes over and governs the rest of the crushing process.

The absorbed energy during the collapse is determined using the so-called SFE theory. Based on this theory, the internal energy is absorbed in certain regions of the sidewalls which undergo large plastic deformations and the rest of the surface (trapezoidal areas in Fig. 2) moves rigidly with no deformation. The total absorbed energy is then the sum of energy contribution from each region shown in Fig. 2; that is, the energies absorbed during quasi-inextensional mode in a toroidal surface denoted by region 1 in Fig. 2(a) with energy value  $E_1$ , horizontal hinge lines denoted by region 2 with energy  $E_2$ , and the inclined traveling hinge lines denoted by region 3 with energy  $E_3$ . Also during extensional mode, energy is absorbed in regions denoted by 4, 5 and 6 which are associated with the two opening conical surfaces with energy  $E_4$ , horizontal hinge lines with energy  $E_5$  and the inclined stationary hinge lines with energy  $E_6$ . Expressions for all these energies have analytically been derived in detail in Appendix 1. There are two sets of variables in this study; (1) – the geometric parameters as the independent variables denoted by  $\chi$  (including shell thickness  $t$ , side wall width  $C$  and corner angle  $\psi_0$ ), and (2)-the collapse variables as dependent variables denoted by  $\xi$  which include the crushing wavelength  $2H$ , curvature radius  $b$  and switching angle  $\bar{\alpha}$ . Stated mathematically;

$$\chi = \{t, C, \psi_0\} \quad (5)$$

$$\xi = \{H, b, \bar{\alpha}\} \quad (6)$$

Now, for the mild steel, the material behavior in plastic region is assumed to obey a linear elastic power law hardening which mathematically states;

$$\sigma(\epsilon) = \sigma_U \left( \frac{\epsilon}{\epsilon_U} \right)^n \quad (7)$$

Eq. (7) fully describes the true stress-strain curve for any mild steel alloy under uniaxial test. Plastic flow stress equivalent to extension ( $\sigma_0^N$ ) and bending-rolling deformations ( $\sigma_0^M$ ) are determined as follow [22]:

$$\sigma_0^N = \frac{1}{\epsilon_m^i} \int_0^{\epsilon_m^i} \sigma(\epsilon) d\epsilon = \frac{\sigma_U}{n+1} \left( \frac{\epsilon_m^i}{\epsilon_U} \right)^n \quad (i=1, 2, 3) \quad (8)$$

$$\sigma_0^M = \frac{2}{(\epsilon_m^i)^2} \int_0^{\epsilon_m^i} \sigma(\epsilon) \epsilon d\epsilon = \frac{2\sigma_U}{n+2} \left( \frac{\epsilon_m^i}{\epsilon_U} \right)^n \quad (i=1, 2, 3) \quad (9)$$

In Eqs. (8) and (9),  $\epsilon_m^i$  represent the maximum plastic strains in each region; namely, toroidal surface 1, horizontal hinges line 2 and the inclined hinge lines 3. These strains may be expressed as [22];

$$\epsilon_m^1 = \frac{t}{2b} \quad (10)$$

$$\epsilon_m^2 = \frac{t}{2H} \quad (11)$$

$$\epsilon_m^3 = \frac{t}{2b} \quad (12)$$

Substituting Eq. (10)-(12) into Eqs. (8) and (9), plastic flow stresses corresponding to each region are obtained. The fully

plastic moments corresponding to each region are also obtained according to the following relation:

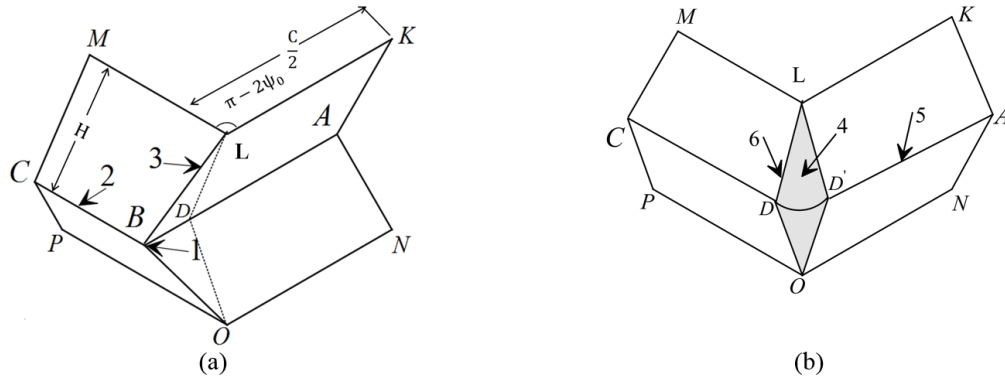


Figure 2. Two different collapse modes a) quasi-inextensional mode b) extensional mode.

$$M_{0i} = \frac{1}{4} \sigma_0^{(i)} t^2 \quad i = 1,2,3 \quad (13)$$

Following a detailed derivation of energies that is given in Appendix 1, to determine the static mean crushing force  $P_{ms}$ , the total internal energy is set equal to the external work  $W_{ext}$  such that;

$$W_{ext} = P_{ms} \delta_{eff} = \sum_{i=0}^6 E_i(\chi, \xi) \quad (14)$$

Here,  $\delta_{eff}$  is the effective crushing distance (length) which is smaller than the whole crushing wavelength  $2H$ , since the shell thickness and radii of curvatures prevent the folds to be completely flattened. Different values have been obtained for  $\delta_{eff}$  in different studies. For the purpose of brevity, instead of a full derivation, referring to Refs. [2-4, 21], one can conclude that for the present collapse mode and parameters ratios  $\frac{c}{t} \geq 6$  and  $\frac{L}{c} \leq 8$ ,  $\frac{\delta_{eff}}{2H} = 0.77$ . In the present study, this value is used for  $\delta_{eff}$  and it turns out that the results are in good agreement with FE findings.

Using extremity condition for  $P_{ms}$  with respect to the collapse variables  $\chi$ , a set of equations are obtained as follows:

$$\frac{\partial P_{ms}}{\partial \chi}(\chi, \xi) = 0 \quad (15)$$

Eq. (15) consists of three nonlinear parametric equations which should be solved to yield the collapse variables and then the mean crushing force in terms of the geometric parameters. Since these equations can not be solved analytically, a detailed procedure for extracting the solutions will be discussed in the following section. In the case of impact loading, to introduce the effect of material strain rate sensitivity, the empirical Cowper-Symonds uniaxial constitutive equation for mild steel is used as follows:

$$\frac{\sigma_{0d}^{(i)}}{\sigma_0^{(i)}} = 1 + \left(\frac{\dot{\epsilon}}{q}\right)^{1/p} \quad i = 1,2,3 \quad (16)$$

This equation is widely used to assess the material strain rate effects in many structures [21, 22]. In this equation,  $p$  and  $q$  are the two constants for which different values are reported in different studies. Values of  $p = 6844$  and  $q = 3.91$  which have been widely used by others, are selected and will be used in the present study. Additionally,  $\sigma_{0d}^{(i)}$  is the dynamic flow stress associated with the  $i^{th}$  plastic region and  $\dot{\epsilon}$  is the strain rate determined as follows:

$$\dot{\epsilon} = \frac{tV_{0k}}{2b\delta_{eff}} \quad (17)$$

Substituting Eq. (17) into Eq. (16), the dynamic plastic flow stress associated with the  $i^{th}$  region is obtained as;

$$\sigma_{0d}^{(i)} = \sigma_0^{(i)} \left[ 1 + \left( \frac{tV_{0k}}{2bq\delta_{eff}} \right)^{1/p} \right] \quad (18)$$

In Eq. (18),  $V_{0k}$  is the velocity of the impactor mass at the beginning of the  $k^{th}$  crushing wavelength. This way, instead of using an average velocity during the whole crushing distance, as assumed by others, a separate velocity in each wavelength is calculated and used. Consequently, based on the impactor velocity, different dynamic mean crushing forces are calculated in the progressive wavelengths, values of which are determined as;

$$P_{mdk} = P_{ms} \left[ 1 + \left( \frac{tV_{0k}}{2bq\delta_{eff}} \right)^{1/p} \right] \quad k=1,2,3,\dots \quad (19)$$

In Eq. (19),  $P_{mdk}$  and  $V_{0k}$  are the current dynamic mean crushing force and initial velocity related to the  $k^{th}$  crushing wavelength. To obtain the next mean dynamic force and the initial velocity, it is assumed that the impactor velocity is reducing linearly during crushing process (the FE results confirms this assumption). Therefore, the acceleration can be taken to be a constant. On this basis, the velocity at the beginning of the next crushing wavelength is obtained stepwise and in an iterative process using the current values through the following equation:

$$V_{0k+1} = \sqrt{V_{0k}^2 - \frac{2P_{mdk}\delta_{eff}}{M}} \quad (20)$$

The process of determining values of  $P_{mdk}$  is repeated until the velocity becomes non-positive i.e.  $V_{0k+1} \leq 0$  (this means that the impactor has stopped). The overall dynamic mean crushing force,  $P_{md}$  (which will be compared with the experimental values of other studies and FE findings of present work), can be obtained by averaging  $P_{mdk}$  values as follows:

$$P_{md} = \sum_{k=1}^N \frac{P_{mdk}}{N} \quad k=1, 2, 3,\dots \quad (21)$$

In Eq. (21),  $N$  is the number of wavelengths ( $2H$ ) and is equal to the number of  $ks$  until the value of  $V_{0k+1}$  becomes negative. Therefore,  $N$  is always an integer and is simply used to obtain the average dynamic crushing force given by Eq. (21). To obtain the real number of folds which may not be an integer, the overall crushing length  $d$  must be divided by the effective crushed length in each wavelength. Therefore, the overall crushed length  $d$  in the column, the absorbed energy  $E_k$  in each crushing wavelength, and the real number of folds  $N_f$  are obtained through the following relations:

$$d = \frac{1}{2} m V_{01}^2 / P_{md} \quad (22)$$

$$E_k = P_{mdk} \delta_{eff} \quad (23)$$

$$N_f = \frac{d}{\delta_{eff}} \quad (24)$$

### 2.4. Solution method

In this section, a solution procedure is proposed for solving the nonlinear algebraic Eq. (15). First, the values of integrals  $I_i$ s in the energy terms  $E_{i_s}$  ( $i = 1, 2, \dots, 6$ ) which have been determined in Appendix 1 are estimated as functions of the crushing angle  $\bar{\alpha}$ . For this purpose, those values of  $I_i$ s which can not be determined

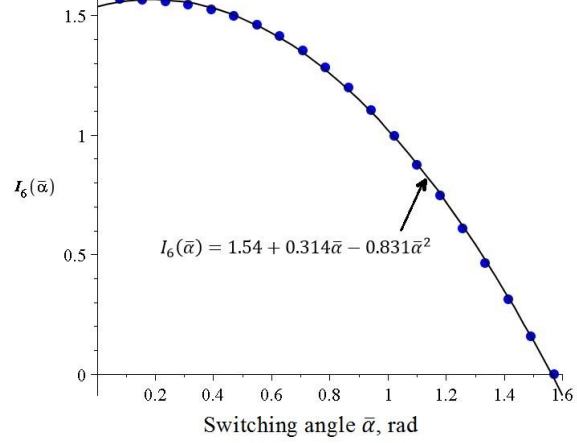
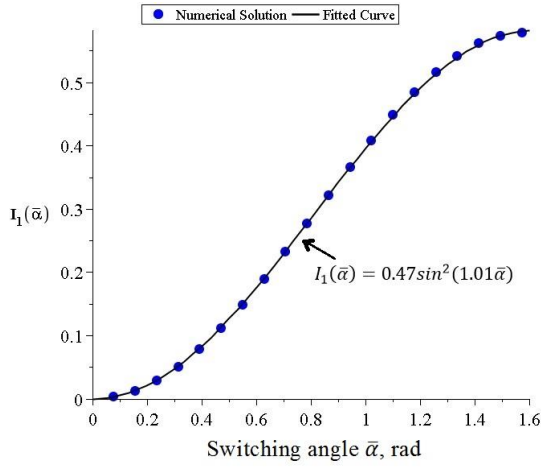


Figure 3. Fitted curves on data points used for numerical calculation of  $I_1$  and  $I_6$ .

On substituting  $I_i$ s into Eq. (15), three nonlinear parametric equations are obtained which are solved numerically for 20 discretized values, for each one of the two parameters  $t$  and  $C$ . Now, the equations are no longer parametric and are only functions of the collapse variables  $\xi$  which could be easily solved 400 times

analytically, are obtained numerically (point-wise) for different and enough values of  $\bar{\alpha}$  ( $0 < \bar{\alpha} < \frac{\pi}{2}$ ) (here twenty points), and then the solution points are fitted into smooth functions using the least square curve fitting algorithm. Among the expressions obtained for  $I_i$ s in Appendix 1,  $I_1$  and  $I_6$  are the ones that must be evaluated numerically. The proper curves fitted to these two functions appear in Fig. 3.

based on 400 different combinations of  $t$  and  $C$ . This way, 400 solution points, for each set of collapse variables  $H$ ,  $\bar{\alpha}$ , and  $b$ , and then the static mean crushing force  $P_{ms}$  are obtained. Figures 4(a) and 4(b) show the variations in crushing forces in a square tube based on the selected values of  $C$  and  $t$  (i.e. for each value of  $\psi_0$ ).

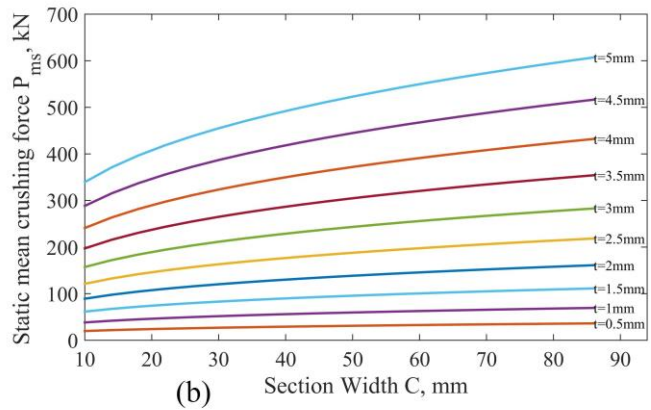
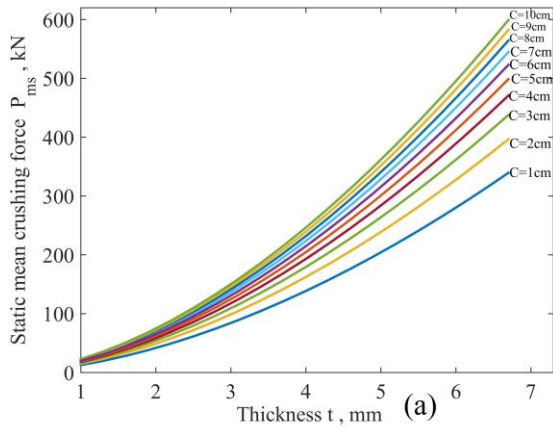


Figure 4. Static mean crushing force for square section; (a) as a function of thickness for different section widths, and (b) as a function of widths for different thicknesses.

Fig.5 shows the three dimensional changes in crushing force as a function of geometric parameters (i.e. thickness and width), based on the foregoing selected points. According to Figs. 5(a) and 5(b), the crushing force  $P_{ms}$  and the crushing length  $H$  highly depend on  $C$  and  $t$ . Obviously, smaller widths  $C$  and thicker wall thicknesses  $t$ , will cause a sudden rise in  $P_{ms}$ . Additionally, due to smooth generated surfaces, it is possible to fit the results to any appropriate function. In this study, polynomial functions of the form  $At^rC^s$  are fitted to the results using the least squares algorithm in Matlab with 95% upper and lower bound confidence for constants  $A$ ,  $r$  and  $s$ .

Variations in  $C$  and  $t$  seem to have similar effects on the curvature radius (see Fig. 5(c)). According to Fig. 5(d), the effects of  $C$  and  $t$  on switching angle  $\bar{\alpha}$  seem to be less, compared to the other plots shown in this figure. However, for a wide range of

square tube geometric parameters, the switching angle  $\bar{\alpha}$  (the angle at which the collapse mode shifts from quasi-inextensional to extensional) is in the range of 84 to 90 degrees. This indicates that the quasi-inextensional collapse mode governs most of the crushing process, and hence, inherits most of the absorbed energy. Also, increasing  $\frac{C}{t}$  ratio, increases  $\bar{\alpha}$  toward 90° (representing a pure quasi-inextensional collapse mode). Similar procedure can be performed on other cross sectional shapes by simply replacing the geometric parameters for the sections shown in Table 1. The corresponding results can be obtained based on successive runs either in Matlab or Maple software. Table 1 includes the fitted polynomial surfaces related to the mean crushing force and collapse variables obtained for columns with different cross sectional shapes.

As mentioned before, due to strain rate effect and reduction in the impactor velocity, different dynamic mean crushing forces

$P_{mdk}$ , associated with different crushing wavelengths, are obtained.

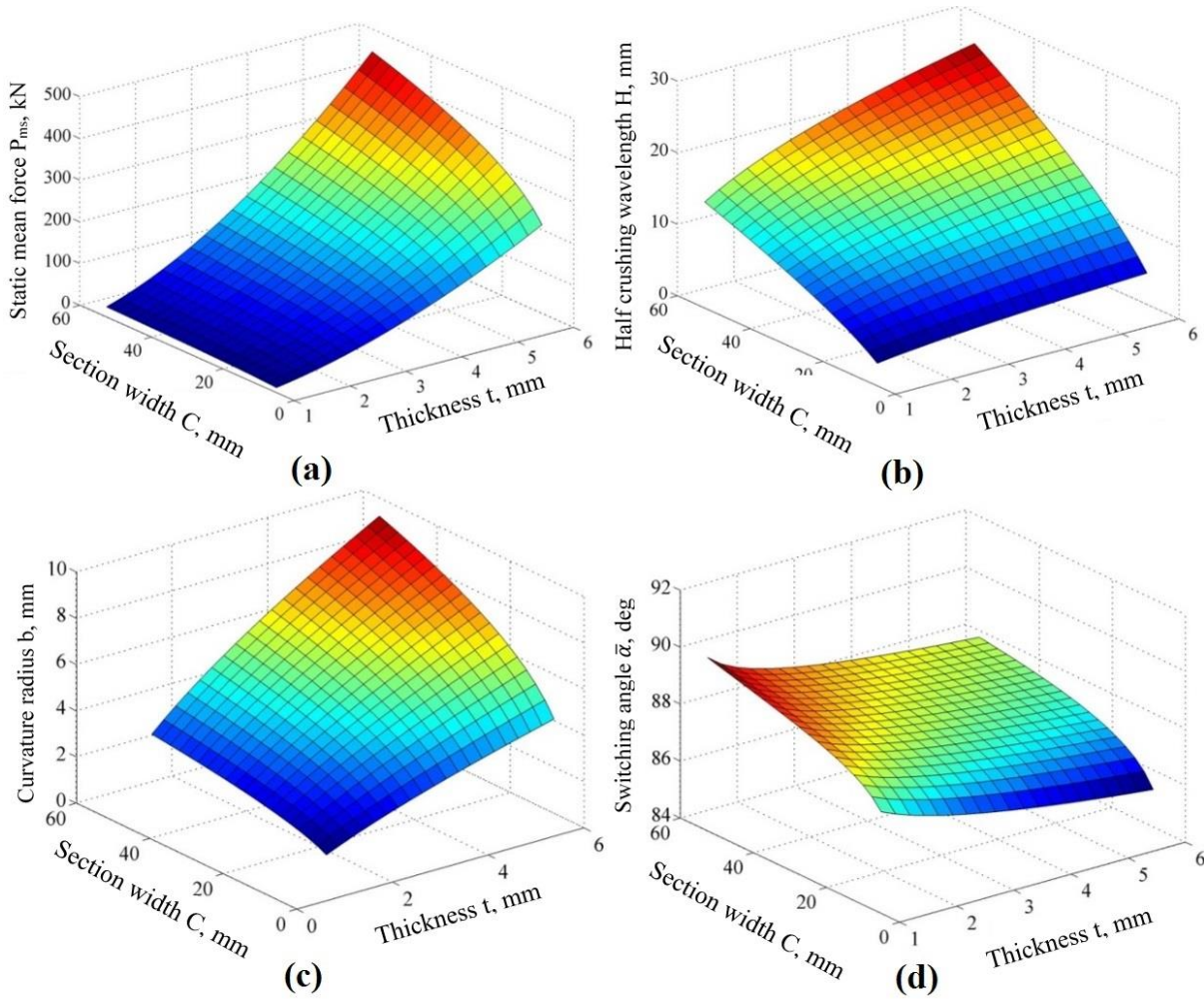
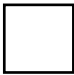

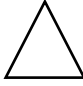


Figure 5. Surfaces of a) static mean crushing force, b) crushing length, c) curvature radius, d) switching angle as a function of geometric parameters

Table 1. Collapse variables for different thin walled columns obtained in present study.

Section	Square tube ( $\psi_0 = \frac{\pi}{4}$ )	Hexagonal tube ( $\psi_0 = \frac{\pi}{6}$ )	Triangular tube ( $\psi_0 = \frac{\pi}{3}$ )
Collapse variables			
$P_{ms}$	$14.25\sigma_0 t^{1.699} C^{0.298}$	$27.07\sigma_0 t^{1.673} C^{0.274}$	$6.80\sigma_0 t^{1.682} C^{0.311}$
H	$1.0921t^{0.342} C^{0.658}$	$0.708t^{0.342} C^{0.658}$	$1.674t^{0.349} C^{0.655}$
b	$0.807t^{0.673} C^{0.327}$	$0.702t^{0.672} C^{0.327}$	$0.955t^{0.676} C^{0.325}$
$\bar{\alpha}$	$1.51t^{-0.011} C^{0.011}$	$1.491t^{-0.006} C^{0.007}$	$1.404t^{-0.04} C^{0.03}$
$P_{mdk}$	$P_{ms} [1 + \left(\frac{tV_{0k}}{2bq\delta_{eff}}\right)^{1/p}]$	$P_{ms} [1 + \left(\frac{tV_{0k}}{2bq\delta_{eff}}\right)^{1/p}]$	$P_{ms} [1 + \left(\frac{tV_{0k}}{2bq\delta_{eff}}\right)^{1/p}]$

According to Ref. [2], the crushing load for a mild steel square tube with a rigid-perfectly plastic behavior is estimated by Eq. (25), while for a model with similar material behavior and considering a mixed collapse mode, this equation is replaced by Eq. (26) [4].

$$P_{ms} = 13.05\sigma_0 t^{1.67} C^{0.33} \quad (25)$$

$$P_{ms} = 12.16\sigma_0 t^{1.63} C^{0.37} \quad (26)$$

Reference [22], which offers a rigid-power law hardening plastic model for the material but does not yet consider a mixed collapse mode, Calculates  $P_{ms}$  according to Eq. (27).

$$P_{ms} = 14.53\sigma_u t^{1.71} C^{0.29} \quad (27)$$

Among these three equations, the results based on Eq. (27) show better agreements with those of present work. This is due to the fact that the material in Ref. [22] is assumed to behave similar

to the one used in present analysis (note that Eq. (27) lacks other aspects introduced in this work).

### 3. Analytical results and FE simulation

To evaluate the applicability of the proposed approach on estimation of the crushing force due to an impact load, properties of AISI1020 mild steel alloy with power law hardening (expressed by Eq. (7) and given in Table 2), are used in the current analysis.

These values were also used by Abramowicz and Jones [21] for generation of their experimental results given in Table 3. Since the results in Table 3 do not show all single aspects of the crushing mechanism which were considered in the present work, a detailed FE simulation on square columns was also performed, using ANSYS and LS-DYNA software programs. The corresponding results of this part are compared with analytical results of present analysis and those of Ref. [21], whenever possible, for validation of final results found in this work.

**Table 2.** Material properties of AISI1020 mild steel alloy.

Property	Density	Elastic modulus	Poisson's ratio	Yield strength	Ultimate strength	Strain at $\sigma_U$	Hardening power n
Value	7870 <sup>kg</sup> / <sub>m<sup>3</sup></sub>	205GPa	0.29	345Mpa	442MPa	0.3	0.1

**Table 3.** Test results on square tube samples reported in Ref. [21]

Sample	Length (mm)	Width (mm)	Thickness (mm)	Impactor Mass (Kg)	Velocity (m/s)	Kinetic energy (KJ)	Crushing length (mm)	Mean force (KN)
B4	47.9	11.44	1.28	16.75	6.47	0.35	14.5	24.13
B5	48.2	11.43	1.28	16.75	7.40	0.46	22.7	20.26
B7	48.3	11.41	1.29	16.75	8.32	0.58	24.0	24.17
C2	100.0	17.05	1.00	77.25	4.62	0.86	52.6	16.43
C3	100.4	17.08	0.98	16.75	9.62	0.78	49.0	15.97
C4	100.2	17.12	0.95	77.25	5.73	1.33	76.7	17.29
C6	97.0	17.08	0.99	16.75	11.27	1.07	66.8	16.08
C8	96.3	17.11	0.98	16.75	11.27	1.07	68.4	15.70
D1	100.0	18.20	0.90	16.75	9.80	0.81	59.0	13.80
D2	100.4	18.16	0.92	77.25	4.62	0.88	66.7	13.14
D5	200.3	18.15	0.92	77.25	5.55	1.26	92.6	13.60
D6	200.0	18.16	0.91	77.25	6.47	1.72	130.5	13.16
D7	48.1	18.18	0.91	16.75	7.58	0.49	34.3	14.20
D8	48.1	18.24	0.91	16.75	6.84	0.40	29.5	13.46
E1	178.1	36.64	1.64	77.25	8.14	2.59	48.3	53.72
E2	178.0	36.45	1.65	135.5	6.11	2.59	48.5	53.39
E3	222.1	36.49	1.63	135.5	9.62	6.46	144.8	44.61
E4	222.0	36.55	1.62	135.5	4.99	1.74	35.9	48.41
E5	268.0	36.45	1.64	77.25	10.09	4.01	97.8	40.99
E6	267.7	36.46	1.64	135.5	6.84	3.26	67.1	48.60
E7	289.0	36.46	1.63	77.25	10.91	4.67	97.0	48.15
E8	288.8	36.42	1.64	135.5	6.84	3.26	63.7	51.13

The square tube samples were categorized in six different groups A, B, C, D, E and F, based on their geometric parameters (i.e. thickness and width of the section). Since this study is concerned with progressive collapse, then, only those samples following this behavior were selected (groups B, C, D, and E). The samples experiencing global buckling (groups A and F) were excluded in this work. It is worth mentioning that the overall mean dynamic crushing force in the experimental tests could be simply obtained by dividing the initial kinetic energy of the impactor by the total crushing distance.

To perform a detailed simulation study on the mild steel square tubes with dimensions and properties given in Tables 2 and 3, both LS-DYNA and ANSYS software programs were used (ANSYS for buckling and LS-DYNA for crushing simulation). In the first stage of the analysis, to account for geometrical imperfections, a linear buckling analysis was carried out to yield enough buckling modes. Combination of the first three buckling modes were

selected for generation of imperfections (using a small scaling factor in the range of 0.03% of the thickness), value of which were imposed on the tubes by updating their new geometry using geometry tools available in ANSYS Workbench. The tubes with the imposed geometric imperfections are shown in Fig. 6. To continue the analysis, the tubes were imported to LS-DYNA module for preprocessing operation, which included meshing and application of load and boundary (initial) conditions. Proper Material models with properties given in Table 2 and strain-rate hardening effect given according to Eq. (16) were selected using 24\_MAT\_PIECEWISE\_LINEAR\_PLASTICITY keyword. The tubes were meshed with proper size elements to yield accurate results. Zero translational boundary conditions were imposed on the lower end edges. AUTOMATIC\_SINGLE\_SURFACE contact type was used for the shell self-contact with friction coefficient of 0.05. To model the impactor, as well as the inertia and velocity, keyword (RIGIDWALL\_PLANAR\_MOVING\_FORCES) was invoked. Fig. 7 shows the final crushed state of the tubes (groups B to E).

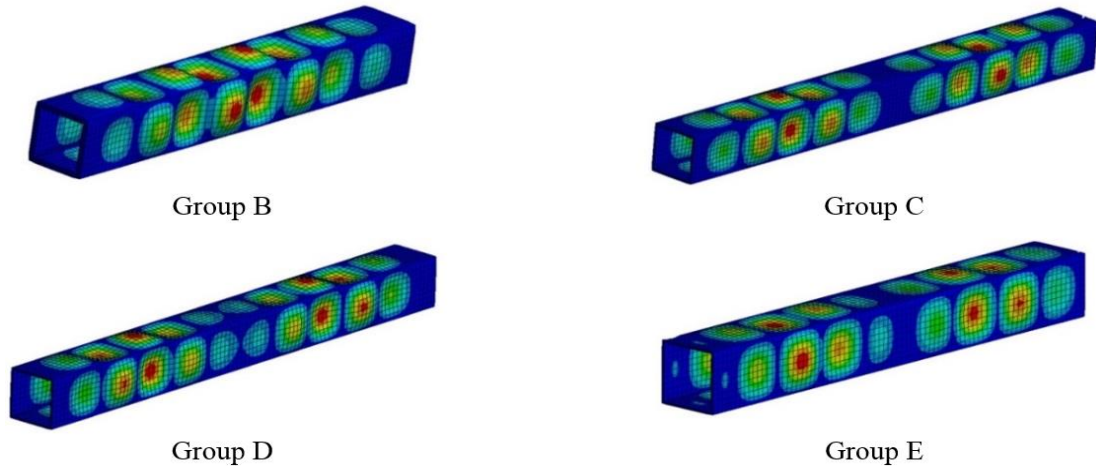


Figure 6. Geometric imperfections embedded through linear buckling analysis of the tubes

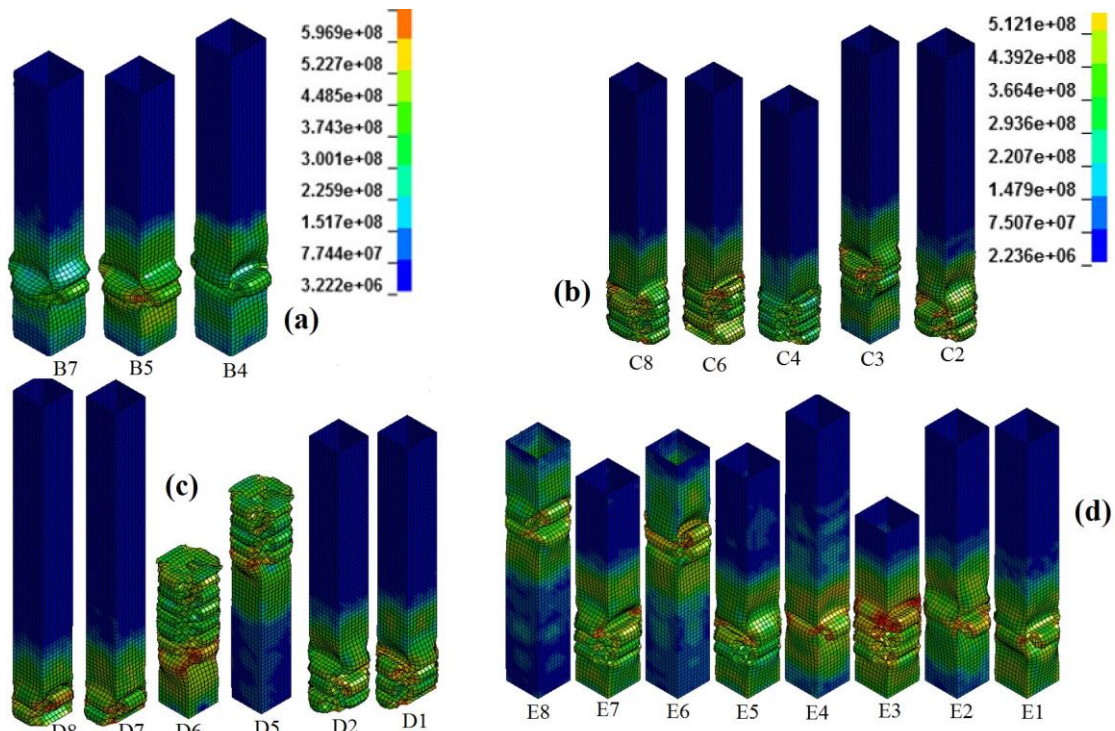


Figure 7. Final crushed state of the square tubes simulated in LS-DYNA, (a) group B, (b) group C, (c) group D, and (d) group E.

As is evident in Fig. 7, the collapse modes are mainly progressively quasi-inextensional. This is in agreement with experimental observations and thus the suggested collapse mode in the previous section is validated. The simulation results on crushing force versus the axial displacement curves for the tubes in groups B to E are shown in Fig. 8. Considering the force-crushing curves for all the tubes, it is observed that unlike the quasi-static loading, the responses to impact loadings are slightly irregular for different wavelengths, yet still enough regular that the bar can be assumed to be crushed in successive similar wavelengths [2- 4]. Additionally, due to strain-rate effects in the material and gradual reduction in impactor velocity, the crushing force decreases during crushing progression. This means that for a more accurate modeling, it is necessary to consider a stepwise mean crushing force corresponding to each crushing wavelength, instead of just a mean force, as has been employed in previous studies [2-4, 21, 22]. Moreover, it is observed that the maximum crushing load occurs at the beginning of the collapse. This is very

important in crashworthiness applications, since in vehicular accidents, it could be a measure of brain and spinal injuries. The area under these curves represent the total absorbed energy which is also equal to the initial kinetic energy of the impactor (since the simulation continues until the impactor completely comes to a halt, and principally all of its energy is converted into internal energy).

Table 4, gives each sample velocity at the beginning of the  $k^{th}$  wavelengths ( $2H$ ), using Eq. (20). In this table, the reduction in mean crushing force is due to strain rate effects and reduction in the impactor velocity. It is worth to mention that the number of steps between the start and stopping periods are not necessarily the number of folds. The real number of wavelengths  $N_f$ , up to the point of stop could be estimated by Eq. (24).

Also, in Table 5, Dynamic mean crushing force for different progressive wavelengths associated with each sample is presented.



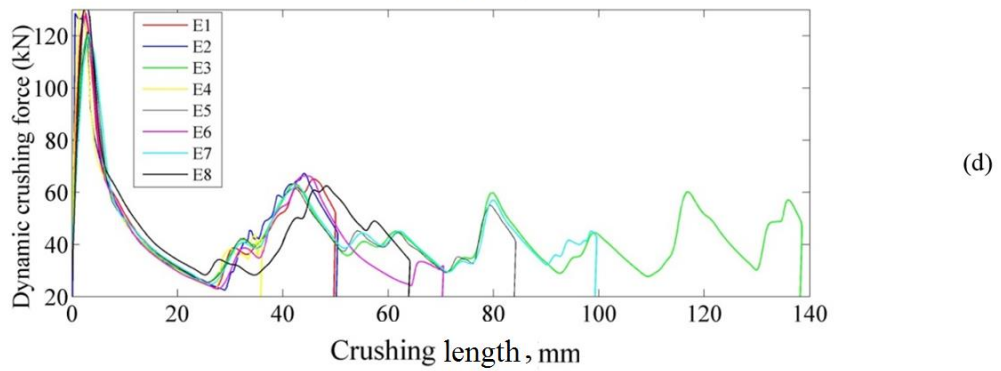
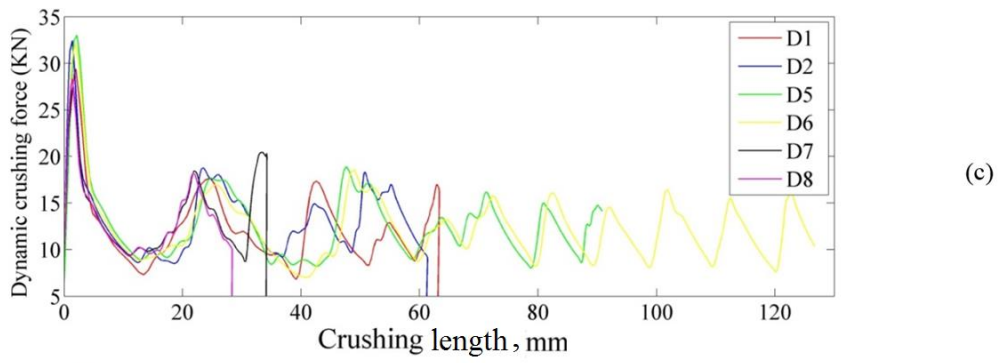
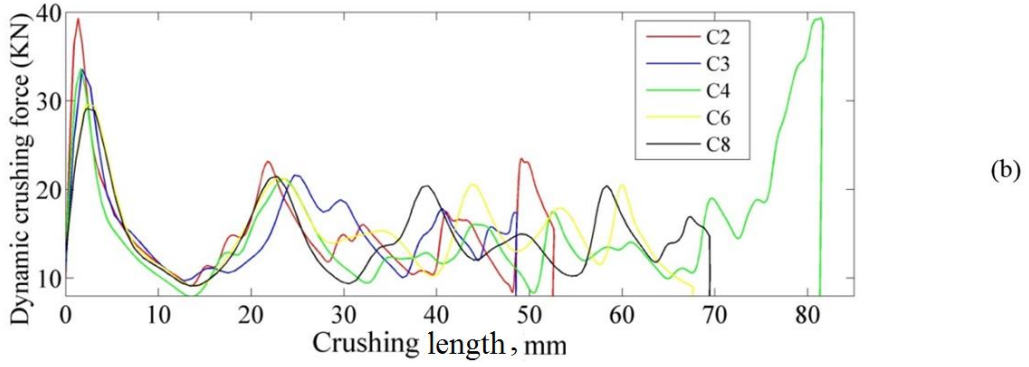
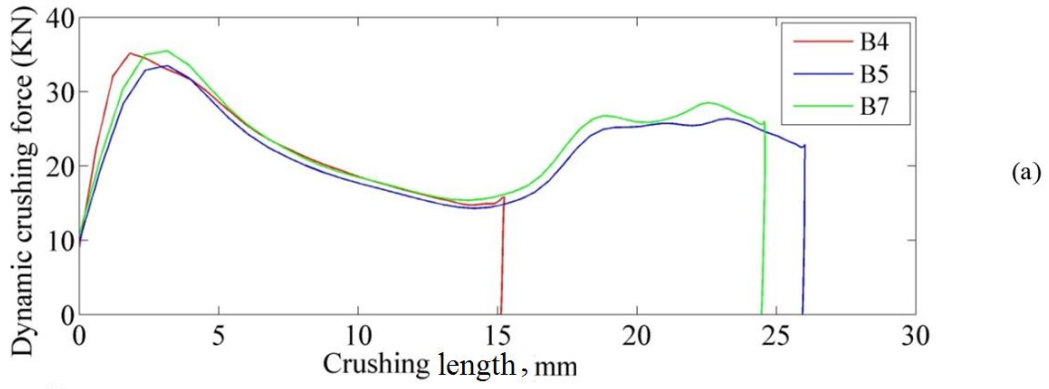


Figure 8. Force vs. crushing length (distance) curves for simulated tube samples in LS-DYNA; (a) Group B, and (b) Group C, (c) Group D, and (d) Group E.

**Table 4.** Number of wavelengths (2H) and the corresponding velocity of each sample at the beginning of each crushing wavelength.

Samples	1 <sup>st</sup> V <sub>0k</sub> (V <sub>01</sub> )(m/s)	2 <sup>nd</sup> V <sub>0k</sub> (V <sub>02</sub> )(m/s)	3 <sup>rd</sup> V <sub>0k</sub> (V <sub>03</sub> )(m/s)	4 <sup>th</sup> V <sub>0k</sub> (V <sub>04</sub> )(m/s)	5 <sup>th</sup> V <sub>0k</sub> (V <sub>05</sub> )(m/s)	6 <sup>th</sup> V <sub>0k</sub> (V <sub>06</sub> )(m/s)	7 <sup>th</sup> V <sub>0k</sub> (V <sub>07</sub> )(m/s)	8 <sup>th</sup> V <sub>0k</sub> (V <sub>08</sub> )(m/s)	9 <sup>th</sup> V <sub>0k</sub> (V <sub>09</sub> )(m/s)	10 <sup>th</sup> V <sub>0k</sub> (V <sub>010</sub> )(m/s)	11 <sup>th</sup> V <sub>0k</sub> (V <sub>011</sub> )(m/s)
B4	6.47	4	0	0	0	0	0	0	0	0	0
B5	7.4	5.35	1.78	0	0	0	0	0	0	0	0
B7	8.32	6.52	4.03	0	0	0	0	0	0	0	0
C2	4.62	4.08	3.45	2.69	1.62	0	0	0	0	0	0
C3	9.62	8.4	6.98	5.22	2.47	0	0	0	0	0	0
C4	5.73	5.34	4.92	4.46	3.95	3.37	2.68	1.73	0	0	0
C6	11.27	10.21	9.04	7.7	6.1	3.93	0	0	0	0	0
C8	11.27	10.23	9.09	7.79	6.24	4.19	0	0	0	0	0
D1	9.8	8.74	7.55	6.15	4.34	0.45	0	0	0	0	0
D2	4.62	4.14	3.59	2.96	2.15	0.72	0	0	0	0	0
D5	5.55	5.15	4.72	4.25	3.72	3.11	2.35	1.2	0	0	0
D6	6.47	6.14	5.78	5.41	5.01	4.58	4.1	3.56	2.94	2.14	0.76
D7	7.58	6.15	4.29	0	0	0	0	0	0	0	0
D8	6.84	5.22	2.82	0	0	0	0	0	0	0	0
E1	8.14	6.29	3.63	0	0	0	0	0	0	0	0
E2	6.11	4.71	2.68	0	0	0	0	0	0	0	0
E3	9.62	8.8	7.9	6.89	5.7	4.22	1.8	0	0	0	0
E4	4.99	3.23	0	0	0	0	0	0	0	0	0
E5	10.09	8.66	6.94	4.67	0	0	0	0	0	0	0
E6	6.84	5.63	4.1	1.46	0	0	0	0	0	0	0
E7	10.91	9.61	8.11	6.29	3.69	0	0	0	0	0	0
E8	6.84	5.64	4.11	1.47	0	0	0	0	0	0	0

**Table 5.** Dynamic mean crushing force for different progressive wavelengths associated with each sample.

Samples	1 <sup>st</sup> P <sub>md</sub> (P <sub>md1</sub> )(KN)	2 <sup>nd</sup> P <sub>md</sub> (P <sub>md2</sub> )(KN)	3 <sup>rd</sup> P <sub>md</sub> (P <sub>md3</sub> )(KN)	4 <sup>th</sup> P <sub>md</sub> (P <sub>md4</sub> )(KN)	5 <sup>th</sup> P <sub>md</sub> (P <sub>md5</sub> )(KN)	6 <sup>th</sup> P <sub>md</sub> (P <sub>md6</sub> )(KN)	7 <sup>th</sup> P <sub>md</sub> (P <sub>md7</sub> )(KN)	8 <sup>th</sup> P <sub>md</sub> (P <sub>md8</sub> )(KN)	9 <sup>th</sup> P <sub>md</sub> (P <sub>md9</sub> )(KN)	10 <sup>th</sup> P <sub>md</sub> (P <sub>md10</sub> )(KN)	11 <sup>th</sup> P <sub>md</sub> (P <sub>md11</sub> )(KN)
B4	23.81	23.04	0	0	0	0	0	0	0	0	0
B5	24.05	23.48	22.1	0	0	0	0	0	0	0	0
B7	24.6	24.12	23.34	0	0	0	0	0	0	0	0
C2	16.82	16.71	16.57	16.38	16.07	0	0	0	0	0	0
C3	17.05	16.88	16.67	16.37	15.78	0	0	0	0	0	0
C4	15.62	15.56	15.49	15.4	15.3	15.19	15.03	14.78	0	0	0
C6	17.56	17.43	17.27	17.07	16.81	16.4	0	0	0	0	0
C8	17.27	17.14	16.98	16.8	16.56	16.18	0	0	0	0	0
D1	14.99	14.86	14.72	14.52	14.24	13.24	0	0	0	0	0
D2	14.83	14.74	14.64	14.51	14.32	13.87	0	0	0	0	0
D5	14.98	14.91	14.84	14.76	14.66	14.54	14.37	14.05	0	0	0
D6	14.84	14.79	14.74	14.68	14.62	14.55	14.46	14.36	14.24	14.06	13.63
D7	14.99	14.8	14.5	0	0	0	0	0	0	0	0
D8	14.91	14.67	14.23	0	0	0	0	0	0	0	0
E1	48.46	47.87	46.84	0	0	0	0	0	0	0	0
E2	48.24	47.72	46.8	0	0	0	0	0	0	0	0
E3	48.33	48.1	47.84	47.52	47.12	46.56	45.35	0	0	0	0
E4	46.4	45.66	0	0	0	0	0	0	0	0	0
E5	48.95	48.55	48.03	47.22	0	0	0	0	0	0	0
E6	48	47.58	46.99	45.58	0	0	0	0	0	0	0
E7	48.66	48.32	47.89	47.32	46.32	0	0	0	0	0	0
E8	47.98	47.57	46.97	45.58	0	0	0	0	0	0	0

Plotting the dynamic mean crushing forces versus the crushing length (distance), showed a stepwise reduction in this force for progressive wavelengths (see Fig. 9). Differences in successive

mean forces depend on the strain rate sensitivity. Although for the mild steel (which is the case in this study) the differences may not be significant in some periods, yet, they may become significant

for materials with higher sensitivity to strain rate. Moreover, the values of dynamic mean crushing force and collapse variables obtained from FE analysis and analytical work of this study are

compared with the experimental results of Ref. [21] on square tubes. This comparison is shown in Table 6 for all sample.

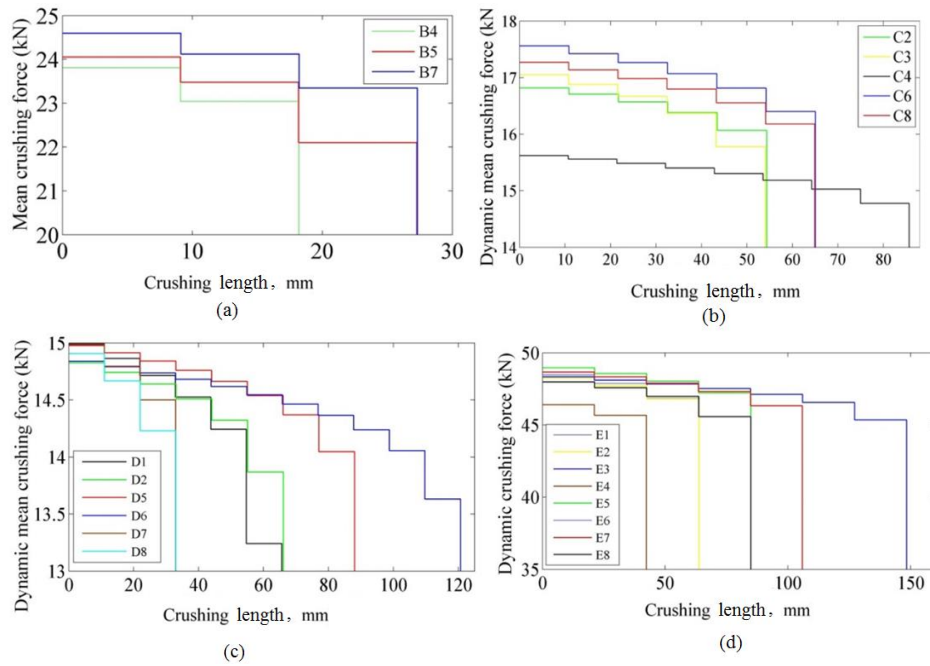


Figure 9. Dynamic mean crushing forces vs. crushing (length) distance for square sections using the approach in present study

Table 6. Comparison between experimental results [21], FEM and the analytical results of present study.

Sample	Experimental $P_{md}$ (KN)	FEM		Analytical					Error percentage (%)		
		FEM crushed distance (mm)	FEM $P_{md}$ (KN)	Curvature radius (b) (mm)	Crushing wavelength (H)	Analytical $P_{ms}$ (KN)	Analytical $P_{md}$ (KN)	crushed distance (mm)	btw. FEM & Analytic	btw. FEM & Experiment	btw. Exprt. & Analytical
B4	24.13	14.8	23.57	2.11	5.91	20.22	23.43	14.96	0.59	2.32	2.9
B5	20.26	20.5	22.43	2.11	5.9	20.22	23.21	19.76	3.48	9.71	11.56
B7	24.17	24.2	23.96	2.12	5.91	20.47	24.02	24.14	0.25	0.87	0.62
C2	16.43	52.9	16.25	2.04	7.06	14.97	16.51	49.94	1.6	1.1	0.49
C3	15.97	48.2	16.18	2.01	7.02	14.47	16.55	46.83	2.29	1.31	3.63
C4	17.29	81.6	16.3	1.97	6.95	13.74	15.3	82.89	6.13	5.73	11.51
C6	16.08	66.1	16.18	2.03	7.04	14.73	17.09	62.24	5.62	0.62	6.28
C8	15.7	68.9	15.53	2.01	7.03	14.48	16.82	63.24	8.31	1.08	7.13
D1	13.8	61.3	13.2	1.94	7.11	12.76	14.43	55.74	9.32	4.35	4.57
D2	13.14	61.3	14.35	1.97	7.15	13.24	14.49	56.9	0.98	9.21	10.27
D5	13.6	91.1	13.83	1.97	7.15	13.24	14.64	81.27	5.86	1.69	7.65
D6	13.16	127.2	13.52	1.95	7.12	13	14.45	111.89	6.88	2.74	9.8
D7	14.2	34.2	14.32	1.96	7.13	13	14.76	32.6	3.07	0.85	3.94
D8	13.46	28.3	14.09	1.96	7.14	13.01	14.6	26.84	3.62	4.68	8.47
E1	53.72	50	51.81	3.65	13.83	43.58	47.72	53.63	7.89	3.56	11.17
E2	53.39	50.4	51.38	3.66	13.81	43.97	47.59	53.15	7.38	3.76	10.86
E3	44.61	138.5	46.63	3.64	13.76	43.08	47.26	132.67	1.35	4.53	5.94
E4	48.41	36.1	48.23	3.62	13.75	42.65	46.03	36.65	4.56	0.37	4.92
E5	40.99	84.2	47.63	3.65	13.78	43.52	48.19	81.6	1.18	16.2	12.57
E6	48.6	70.5	46.24	3.65	13.78	43.52	47.04	67.38	1.73	4.86	3.21
E7	48.15	99.5	46.9	3.63	13.76	43.07	47.7	96.38	1.71	2.6	0.93
E8	51.13	64.1	50.84	3.65	13.77	43.5	47.03	67.4	7.49	0.57	8.02

According to this table, although there are a few cases in which the percentage differences between the results are higher than 4,

yet, there still remain excellent agreements with experimental results on majority of remaining samples used in both studies. This

demonstrates that the current analytical approach can predict the axial collapse of multi-corner thin-walled metal sections under an axial impact with a good accuracy. The advantages of the current proposed analytical approach over the experimental and FEM is the easiness and accuracy of the method due to its explicit closed form solutions for all collapse variables. Obviously, this method may be used for any section with any sectional parameter.

#### 4. Conclusion

In this paper, progressive collapse of thin walled metal columns under quasi-static and impact axial load was investigated in detail via a novel approach to derive the explicit relations for dynamic and static mean crushing forces and collapse variables in terms of geometrical and mechanical properties. SFE theory which is an efficient approach was employed and developed by considering some important effects which have not been considered in previous studies since they lead to parametric equations without a general analytic solution. To overcome this barrier, a semi-analytical procedure was proposed in terms of a series of point-wise solutions, and fitting the proper curves through the resulting data. To accomplish this task, the geometric parameters (i.e. thickness  $t$  and width  $C$  of each section (triangle, square, hexagon)) were discretized into a wide range of  $\frac{t}{C}$  ratios. To attain a solution, 400 combinations of  $(t, C)$  were selected and then, the set of equations were solved numerically at each point. The results were fitted with the simplest possible polynomial curves using the least square error curve fitting method. The generated polynomial functions,  $At^rC^s$ , were used to approximate the results for a wide range of  $t$  and  $C$ , with 95% confidence for the lower and upper bounds for the constants  $A$ ,  $r$  and  $s$ . Instead of using one mean crushing force (for dynamic loading) through the whole crushing distance, a series of stepwise valued mean crushing forces, each corresponding to a crushing wavelength, were obtained and then implemented by considering the strain rate effect and evaluating the velocity reduction of the impactor. The overall dynamic mean force and crushing distances which were obtained through this process were compared with FE and experimental work of others and showed an average error of 4.15% and standard deviation of 2.88. This indicates the applicability of the proposed approach for accurate estimation of the crushing force and length in single walled metal columns.

#### 5. Appendix. 1

This appendix summarizes the procedure of deriving the energies  $E_{i,s}$  in Section 2.2 previously discussed. It should be noted the crushing mechanism is one DOF because it is uniquely designated by the time-like parameter  $\alpha$ . According to Fig.A1:

$$\tan \gamma = \frac{\tan \psi_0}{\sin \alpha} \quad (A1)$$

$$\tan \beta = \frac{\tan \alpha}{\sin \psi_0} \quad (A2)$$

$$\Delta = 2H(1 - \cos(\alpha)) \quad (A3)$$

$$S = H \sin(\alpha) \quad (A4)$$

In which  $\Delta$  is the crushed length between points K and N.

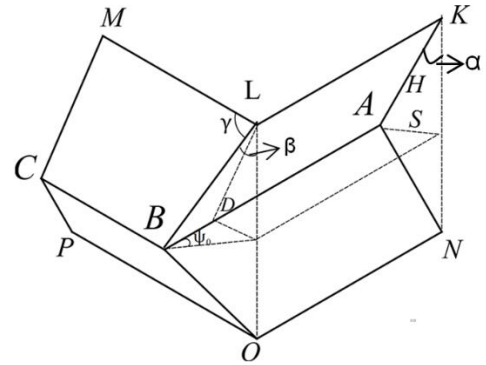


Figure A1. Collapse geometry of the crushing element

The crushing velocity and horizontal velocity of point A are as follows:

$$\dot{\Delta} = 2H\dot{\alpha} \sin \alpha \quad (A5)$$

$$V = \dot{S} = H\dot{\alpha} \cos \alpha \quad (A6)$$

The total rate of absorbing internal energy is governed by the following equation:

$$\dot{E}_{in} = \iint (M_{\alpha\beta} \dot{\kappa}_{\alpha\beta} + N_{\alpha\beta} \dot{\epsilon}_{\alpha\beta}) dS + \sum_1^m M_{oi} \dot{\theta}_i dl^i \quad (A7)$$

In Which  $S$  is the shell surface under continuous plastic deformation field such as the toroidal surface (point B) or the extensional conical surfaces in extensional collapse mode (Fig.4b).  $M_{\alpha\beta}$  and  $N_{\alpha\beta}$  are general in-plane moment and forces,  $\dot{\kappa}_{\alpha\beta}$  and  $\dot{\epsilon}_{\alpha\beta}$  are corresponding curvature and extensional rate respectively,  $M_{oi}$  is plastic moment in discontinuous deformation fields such as horizontal and inclined hinge lines,  $dl^i$  is the line element length,  $\dot{\theta}_i$  is the angular velocity in hinge lines and  $m$  is the number of hinge lines. To determine the energy absorbed in the toroidal surface, a local coordinate system is supposed at point B as shown in Fig.A2 with in-plane components  $\{\theta, \phi\}$ . Neglecting the shear components, the extension and curvature rate tensors are [2-4]:

$$\dot{\lambda} = \begin{bmatrix} \dot{\lambda}_{\phi\phi} & 0 \\ 0 & \dot{\lambda}_{\theta\theta} \end{bmatrix} = \begin{bmatrix} -\frac{\dot{\theta}b \sin \theta}{r} & 0 \\ 0 & 0 \end{bmatrix} \quad (A8)$$

$$\dot{\kappa} = \begin{bmatrix} \dot{\kappa}_{\phi\phi} & 0 \\ 0 & \dot{\kappa}_{\theta\theta} \end{bmatrix} = \begin{bmatrix} \frac{\dot{\theta}a \sin \theta}{r^2} & 0 \\ 0 & \frac{V_t}{b} \end{bmatrix} \quad (A9)$$

In which  $r$  is the toroidal radius defined as  $r = a + b \sin \theta$  which  $a$  and  $b$  are minor and major radii of the toroid surface.

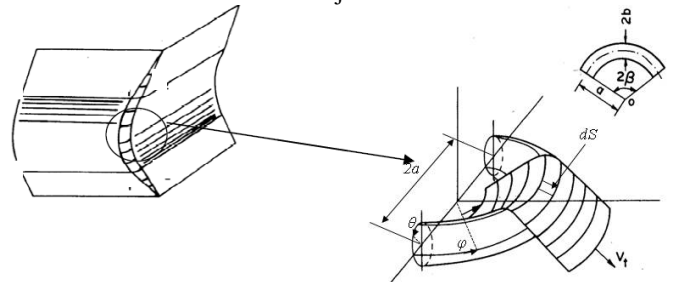


Figure A2. Radial flow of shell over toroidal surface

The tangential velocity of sheet metal flow passing over the toroidal surface is as follows:

$$V_t = \dot{\theta}b = \frac{V}{\tan \psi_0} = \frac{H\dot{\alpha} \cos \alpha}{\tan \psi_0} \quad (A10)$$

The differential element of the area is:

$$dS = b d\theta r d\phi \quad (A11)$$

Upper and lower bounds of the toroidal surface angles during collapse:

$$\begin{cases} \frac{\pi}{2} - \psi < \theta < \frac{\pi}{2} + \psi \\ -\beta < \phi < \beta \end{cases} \quad (A12)$$

In which  $\psi$  is assumed to linearly varying from  $\psi_0$  to  $\frac{\pi}{2}$  as follows:

$$\psi = \psi_0 + \frac{\pi - 2\psi_0}{\pi} \phi \quad (A13)$$

Therefore the energy dissipated in the toroidal surface by considering the integral bounds and substituting into Eq. A (7) is as follows:

$$\begin{aligned} E_1 &= \int_0^{\bar{\alpha}} \left\{ \int_{-\beta}^{\beta} \left[ M_{01} \frac{\hat{\theta} a \sin \theta}{r^2} + N_{01} \frac{\hat{\theta} b \sin \theta}{r} \right] r d\theta \right\} d\phi d\alpha \\ &= \int_0^{\bar{\alpha}} \left\{ \int_{-\beta}^{\beta} \left[ 2\hat{\theta} b^2 N_{01} \sin \psi + \hat{\theta} b M_{01} \frac{1}{\eta} \text{Ln} \left( \frac{1 + \eta \sin \psi}{1 - \eta \sin \psi} \right) \right] d\phi \right\} d\alpha \end{aligned} \quad (A14)$$

In Eq. (A14), subindex 1 indicates toroidal surface and  $M_{01}$  and  $N_{01}$  are corresponding moment and force defined by Eq. (13) and  $\eta = \frac{b}{a}$  which is relatively small assuming thickness constant as in the case of our study i.e.  $\eta \ll 1$  and using Tailor Series expansion [2]:

$$\begin{aligned} E_1(\chi, \xi) &= \int_0^{\bar{\alpha}} \int_{-\beta}^{\beta} \{ 2\hat{\theta} b \sin \psi [N_{01} b + M_{01}] \} d\phi d\alpha \\ &= \frac{4M_{01}H}{t} (4b + t) I_1 \end{aligned} \quad (A15)$$

$$I_1 = \frac{\pi}{\pi - 2\psi_0} \cos \psi_0 \int_0^{\bar{\alpha}} \cos \alpha \sin \left( \frac{\pi - 2\psi_0}{\pi} \beta \right) d\alpha \quad (A16)$$

The contribution of horizontal hinge lines in dissipating energy considering four hinge lines per element:

$$E_2(\chi, \xi) = \int_0^{\bar{\alpha}} \left\{ 4 \int_{-\frac{c}{2}}^{\frac{c}{2}} M_{02} dl \right\} d\alpha = 4M_{02} C \bar{\alpha} \quad (A17)$$

The energy dissipation rate in the two inclined hinge lines which are travelling during collapse so consist of a bending and unbending is as follows:

$$\dot{E}_3 = 2M_0 L \dot{\theta} = 4M_{03} \frac{H^2}{b} \frac{1}{\tan \psi_0} \frac{\cos \alpha}{\sin \gamma} \quad (A18)$$

In which L is the length of two inclined hinge lines equal to:

$$L = \frac{2H}{\sin \gamma} \quad (A19)$$

And the energy dissipated in inclined hinge lines in quasi-inextensional collapse mode:

$$E_3(\chi, \xi) = \int_0^{\bar{\alpha}} \dot{E}_3 d\alpha = 4M_{03} \frac{H^2}{b} I_3 \quad (A20)$$

$$I_3 = \frac{1}{\tan \psi_0} \int_0^{\bar{\alpha}} \frac{\cos \alpha}{\sin \gamma} d\alpha \quad (A21)$$

For determining energy dissipation in extensional collapse mode (Fig.4b), one can refer to reference [4]. This mode begins with forming two extending conical surfaces, so the extension energy rate is as follows:

$$\dot{E}_4 = \iint N_{01} \dot{\lambda}_{\theta\theta} dS = 4M_{01} V_t \frac{H}{b} \quad (A22)$$

$V_t$  is the velocity tangent to conical surface is stated as follows:

$$V_t = \frac{H}{\sin^2 \gamma} \dot{\gamma} \quad (A23)$$

Substituting Eq. (A23) into (A22) and doubling the result for there are two such conical surfaces:

$$E_4(\chi, \xi) = 8M_{01} \frac{H^2}{t} I_4 \quad (A24)$$

$$I_4 = \int_{\bar{\alpha}}^{\alpha_f} \frac{d\gamma}{\sin^2 \gamma} = \int_{\bar{\alpha}}^{\alpha_f} \frac{d(\tan^{-1}(\frac{\tan \psi_0}{\sin \alpha}))}{\sin^2(\tan^{-1}(\frac{\tan \psi_0}{\sin \alpha}))} \quad (A25)$$

The energy dissipation due to horizontal hinge lines in extensional collapse mode:

$$E_5(\chi, \xi) = 4M_{02} C(\alpha_f - \bar{\alpha}) \quad (A26)$$

And finally energy dissipation due to the inclined hinge lines in extensional collapse mode by determining  $\hat{\theta}$  [4]:

$$\dot{E}_6 = M_{03} L 2\dot{\theta} = 2M_{03} H \frac{\sin \alpha (\sin^2 \alpha + \tan^2 \psi_0)}{\tan \psi_0 (\sin^2 \alpha + \tan \psi_0 \sin^2 \alpha)} \quad (A27)$$

$$E_6(\chi, \xi) = 2M_{03} H I_6(\psi_0, \bar{\alpha}, \alpha_f) \quad (A28)$$

$$I_6 = \frac{2}{\tan \psi_0} \int_{\bar{\alpha}}^{\alpha_f} \frac{\sin \alpha (\sin^2 \alpha + \tan^2 \psi_0)}{\sin^2 \alpha + \tan \psi_0 \sin^2 \alpha} d\alpha \quad (A29)$$

## 7. References

- [1] J. Alexander, An approximate analysis of the collapse of thin cylindrical shells under axial loading, *The Quarterly Journal of Mechanics and Applied Mathematics*, Vol. 13, No. 1, pp. 10-15, 1960.
- [2] T. Wierzbicki, W. Abramowicz, On the crushing mechanics of thin-walled structures, *Journal of Applied mechanics*, Vol. 50, No. 4a, pp. 727-734, 1983.
- [3] W. A. N. Jones, W. Abramowicz, Dynamic axial crushing of square tubes, *International Journal of Impact Engineering*, Vol. 2, pp. 179-208, 1984.
- [4] W. Abramowicz, T. Wierzbicki, Axial crushing of multicorner sheet metal columns, *Journal of Applied Mechanics*, Vol. 56, No. 1, pp. 113-120, 1989.
- [5] M. White, N. Jones, W. Abramowicz, A theoretical analysis for the quasi-static axial crushing of top-hat and double-hat thin-walled sections, *International Journal of Mechanical Sciences*, Vol. 41, No. 2, pp. 209-233, 1999.
- [6] A. Najafi, M. Rais-Rohani, Mechanics of axial plastic collapse in multi-cell, multi-corner crush tubes, *Thin-Walled Structures*, Vol. 49, No. 1, pp. 1-12, 2011.
- [7] W. Hao, J. Xie, F. Wang, Theoretical prediction of the progressive buckling and energy absorption of the sinusoidal corrugated tube subjected to axial crushing, *Computers & Structures*, Vol. 191, pp. 12-21, 2017.
- [8] W. Hong, F. Jin, J. Zhou, Z. Xia, Y. Xu, L. Yang, Q. Zheng, H. Fan, Quasi-static axial compression of triangular steel tubes, *Thin-Walled Structures*, Vol. 62, pp. 10-17, 2013.
- [9] G. Martínez, C. Graciano, P. Teixeira, Energy absorption of axially crushed expanded metal tubes, *Thin-Walled Structures*, Vol. 71, pp. 134-146, 2013.
- [10] T. Wierzbicki, W. Abramowicz, The mechanics of deep plastic collapse of thin walled structures, *Jones N, Wierzbicki T, editors. Structural failure*, pp. 281-329, 1989.
- [11] X. Zhang, H. Huh, Crushing analysis of polygonal columns and angle elements, *International Journal of Impact Engineering*, Vol. 37, No. 4, pp. 441-451, 2010.
- [12] X. Zhang, H. Zhang, Crush resistance of square tubes with various thickness configurations, *International Journal of Mechanical Sciences*, Vol. 107, pp. 58-68, 2016.
- [13] J. Song, Y. Zhou, F. Guo, A relationship between progressive collapse and initial buckling for tubular structures under axial loading, *International Journal of Mechanical Sciences*, Vol. 75, pp. 200-211, 2013.
- [14] S. Liu, Z. Tong, Z. Tang, Y. Liu, Z. Zhang, Bionic design modification of non-convex multi-corner thin-walled columns for improving energy absorption through adding bulkheads, *Thin-Walled Structures*, Vol. 88, pp. 70-81, 2015.
- [15] Y. Tao, S. Duan, W. Wen, Y. Pei, D. Fang, Enhanced out-of-plane crushing strength and energy absorption of in-plane graded honeycombs, *Composites Part B: Engineering*, Vol. 118, pp. 33-40, 2017.
- [16] M. Macaulay, R. Redwood, Small scale model railway coaches under impact, *The Engineer*, Vol. 218, pp. 1041-1046, 1964.

- [17] A. Pugsley, The crumpling of tubular structures under impact conditions, in *Proceeding of*, 33-41.
- [18] A. Coppa, New ways to soften shock, *Machine Design*, Vol. 28, pp. 130-140, 1968.
- [19] A. A. Ezra, An assessment of energy absorbing devices for prospective use in aircraft impact situations, in *Proceeding of*, Pergamon Press, pp.
- [20] S. Reid, T. Reddy, *Axially loaded metal tubes as impact energy absorbers*, in: *Inelastic behaviour of plates and shells*, Eds., pp. 569-595: Springer, 1986.
- [21] W. Abramowicz, N. Jones, Dynamic progressive buckling of circular and square tubes, *International Journal of Impact Engineering*, Vol. 4, No. 4, pp. 243-270, 1986.
- [22] W. Abramowicz, Thin-walled structures as impact energy absorbers, *Thin-Walled Structures*, Vol. 41, No. 2, pp. 91-107, 2003.
- [23] J. Fang, Y. Gao, G. Sun, N. Qiu, Q. Li, On design of multi-cell tubes under axial and oblique impact loads, *Thin-Walled Structures*, Vol. 95, pp. 115-126, 2015.
- [24] H. Sun, J. Wang, G. Shen, P. Hu, Energy absorption of aluminum alloy thin-walled tubes under axial impact, *Journal of Mechanical Science and Technology*, Vol. 30, No. 7, pp. 3105-3111, 2016.
- [25] D. Karagiozova, M. Alves, Dynamic elastic-plastic buckling of structural elements: a review, *Applied Mechanics Reviews*, Vol. 61, No. 4, pp. 040803, 2008.
- [26] T. Tran, S. Hou, X. Han, M. Chau, Crushing analysis and numerical optimization of angle element structures under axial impact loading, *Composite Structures*, Vol. 119, pp. 422-435, 2015.
- [27] C. Zhou, B. Wang, J. Ma, Z. You, Dynamic axial crushing of origami crash boxes, *International journal of mechanical sciences*, Vol. 118, pp. 1-12, 2016.
- [28] M. Costas, J. Díaz, L. Romera, S. Hernández, A multi-objective surrogate-based optimization of the crashworthiness of a hybrid impact absorber, *International Journal of Mechanical Sciences*, Vol. 88, pp. 46-54, 2014.
- [29] S. Ebrahimi, N. Vahdatzad, Multiobjective optimization and sensitivity analysis of honeycomb sandwich cylindrical columns under axial crushing loads, *Thin-Walled Structures*, Vol. 88, pp. 90-104, 2015.
- [30] A. Jusuf, T. Dirgantara, L. Gunawan, I. S. Putra, Crashworthiness analysis of multi-cell prismatic structures, *International Journal of Impact Engineering*, Vol. 78, pp. 34-50, 2015.
- [31] A. P. Meran, T. Toprak, A. Muğan, Numerical and experimental study of crashworthiness parameters of honeycomb structures, *Thin-Walled Structures*, Vol. 78, pp. 87-94, 2014.
- [32] M. Bambach, M. Elchalakani, Plastic mechanism analysis of steel SHS strengthened with CFRP under large axial deformation, *Thin-walled structures*, Vol. 45, No. 2, pp. 159-170, 2007.
- [33] A. Farajpour, A. Rastgoo, M. Farajpour, Nonlinear buckling analysis of magneto-electro-elastic CNT-MT hybrid nanoshells based on the nonlocal continuum mechanics, *Composite Structures*, Vol. 180, pp. 179-191, 2017.
- [34] A. Rajaneesh, I. Sridhar, S. Rajendran, Relative performance of metal and polymeric foam sandwich plates under low velocity impact, *International Journal of Impact Engineering*, Vol. 65, pp. 126-136, 2014.
- [35] L. Aktay, A. K. Toksoy, M. Güden, Quasi-static axial crushing of extruded polystyrene foam-filled thin-walled aluminum tubes: experimental and numerical analysis, *Materials & design*, Vol. 27, No. 7, pp. 556-565, 2006.
- [36] M. Shishesaz, M. Kharazi, P. Hosseini, M. Hosseini, Buckling Behavior of Composite Plates with a Pre-central Circular Delamination Defect under in-Plane Uniaxial Compression, *Journal of Computational Applied Mechanics*, Vol. 48, No. 1, pp. 12, 2017.
- [37] B. W. Schafer, The direct strength method of cold-formed steel member design, *Journal of constructional steel research*, Vol. 64, No. 7-8, pp. 766-778, 2008.
- [38] B. Schafer, Local, distortional, and Euler buckling of thin-walled columns, *Journal of structural engineering*, Vol. 128, No. 3, pp. 289-299, 2002.
- [39] S. P. Timoshenko, Stability of bars, plates, and shells, *International Applied Mechanics*, Vol. 7, No. 10, pp. 1175-1176, 1971.

### Nomenclature

A	Constant of curve-fitting	$N_f$	Number of wavelengths (folds)
$A_g$	Gross cross section of the column	$\chi(t, C, \psi_0)$	Geometric parameters
b	Radius of curvature	$\xi(H, b, \bar{\alpha})$	Collapse variables
$\alpha, \beta, \gamma$	Angles of crushing mechanism in Fig. A1	$P_{cr}$	Critical buckling load
c	Width of the section	$P_{ult}$	Ultimate buckling load
d	Overall crushing length	$P_Y$	Yield load
$\delta_{eff}$	Effective crushing length of each fold	$P_{ms}$	Static mean crushing force
$\Delta$	Axial crushing length	$P_{mdk}$	Dynamic mean crushing force associated with $k^{th}$ crushing wavelength
E	Modulus of elasticity	$P_{md}$	Overall dynamic mean crushing force
$E_0$	Elastic absorbed energy	p, q	Constants in Cowper-Symond model
$E_i$	Plastic absorbed energy of the $i^{th}$ region ( $i=1, \dots, 6$ )	$\phi, \psi, \theta$	Angles used in crushing analysis in Fig. A1
$\epsilon_U$	Ultimate strain	$\psi_0$	Corner angle
$\dot{\epsilon}$	Strain rate	$\sigma_U$	Ultimate strength
H	Half crushing wavelength	$\sigma_Y$	Yield strength
$I_i$	Integrals values associated with $i^{th}$ region ( $i=1, \dots, 6$ )	$\sigma_0^N$	Extensional flow stress
$k_c$	Buckling coefficient	$\sigma_0^M$	Bending-rolling flow stress
$\kappa, \dot{\kappa}$	Curvature and curvature rate	$\sigma_0^i$	Flow stress of the $i^{th}$ region ( $i=1, \dots, 6$ )
L	Length of the column	r, s	Constants of curve-fitting
M	Mass of the impactor	t	Thickness of column plates
$M_{0i}$	Plastic moment associated with $i^{th}$ region ( $i=1, \dots, 6$ )	v	Poisson's ratio
n	Power law hardening coefficient		